Fullerides

DOI: 10.1002/ange.201305808

Counterintuitive Anisotropy of Electron Transport Properties in $KC_{60}(THF)_5 \cdot 2THF$ Fulleride**

*A. Kromer, U. Wedig, E. Roduner, M. Jansen, and Konstantin Yu. Amsharov**

The discovery of unique physical properties possessed by alkali metal fullerides A_xC_{60} ($x = 1$–3, A = K, Rb, Na, Cs) such as conductivity and superconductivity has prompted intensive investigation in recent years with regards to these materials.[1] Nevertheless, the exact nature of the electronic properties exhibited by fulleride-based solids is not yet fully clarified and still remains a much discussed subject in many research groups worldwide. As a basis for the deeper understanding of fulleride properties and the further elaboration of a structure–property relationship, detailed knowledge of their structural features is indispensable. Single-crystal X-ray structure determination is the most powerful experimental technique for detailed structural analysis; unfortunately, progress in this field with respect to fulleride characterization has been slow because of difficulties in the synthesis of high-quality single crystals containing fullerene anions. As a rule, the fulleride crystals are twinned and frequently suffer orientation disorder of the sphere-like C_{60} anions.[2] Moreover, the strong tendency of C_{60} anion radicals to recombine and form diamagnetic single-bonded $(C_{60})_2^{2-}$ ions,[3] has further impaired the ability to obtain the requisite close-packed $C_{60}^{\bullet-}$ structures essential for manifestation of conductivity. As a matter of fact, only a few high-quality structures have been reported to date, where individual C_{60} anion radicals have remained separated at low temperatures.[4] Recently, a 2D-layered structure in which C_{60} anion radicals form a 2D honeycomb sublattice with short fullerene-to-fullerene distances has been reported and investigated.[5] The compound was found to be a fascinating example of the first fullerene-based two-dimensional organic metal to be described. In contrast, a later reported 2D-layered structure of $CsC_{60}(THF)_4$ comprising layers of an atypical square-shaped configuration of fully ordered fullerene anion radicals with short C_{60}–C_{60} center-to-center distances has shown no sign of conductivity.[6] These findings clearly point to the importance of the relative orientational configuration of fullerene anions in the crystal for manifestation of conductivity phenomena in the solid state.

Herein, we report the combined results of investigations into the electronic and structural properties of $KC_{60}(THF)_5 \cdot 2THF$ single crystals. The title compound exhibits a unique 2D arrangement of C_{60} anion radicals, in which corrugated layers are formed with close fullerene–fullerene contacts. Important findings include the presence of one-dimensional electric conductivity and the observation of a counterintuitive anisotropy for electron transport. A detailed crystallographic and spectroscopic study carried out with individual single crystals, together with quantum chemical calculations, reveals the main factors responsible for effective interactions between fullerene anions leading to the manifestation of conductivity in fullerides.

The C_{60} anion radicals were obtained from solid C_{60} in a THF/octane mixture by reduction with metallic Zn in the presence of potassium hydroxide using an all-glass system according to a previously reported procedure.[6,7] The fulleride crystals were grown in a sealed glass ampoule under inert gas by a gradient solvent exchange process. $KC_{60}(THF)_5 \cdot 2THF$ crystallized as black lustrous needle-like crystals of up to 6 mm length. The compound was found to be relatively unstable under exposure to air for several days. Accordingly, all sample preparation and manipulation was carried out under anaerobic conditions. The crystal structure of $KC_{60}(THF)_5 \cdot 2THF$ was determined from single-crystal data recorded at 260, 200, 100, and 50 K. A complete description of the structure at 100 K is available elsewhere.[7] Briefly, the $KC_{60}(THF)_5 \cdot 2THF$ crystallized in the orthorhombic space group $Pca2_1$ with four formula units per unit cell. At room temperature, the C_{60} anion radicals displayed rotational disorder. Full ordering of the $C_{60}^{\bullet-}$ species took place below 240 K, followed by structural transformation into an orthorhombic space group $P2_12_12$. The C_{60} anion radicals were found to form corrugated layers with short center-to-center fullerene distances in the *a*–*c* crystallographic plane. The intralayer center-to-center fullerene distances at 100 K were found to be 10.15 Å along the *a* axis and 9.85 Å along the *c* axis. The negative charges of C_{60} anion radicals are compensated by cationic $[K(THF)_5]^+$ building units which separate the above discussed fullerene layers with an interlayer spacing of 15.06 Å along the *b* axis (Figure 1).

Electron spin resonance (ESR) measurements were performed for individual single crystals differently orientated relative to the external magnetic field; investigations revealed substantial features and direction-dependent changes of line shapes. Below 40 K, the obtained X-band ESR spectra showed typical resonances of $C_{60}^{\bullet-}$ with a single Lorentzian line located near the free electron *g* factor. Numerical

[*] Dr. U. Wedig, Prof. M. Jansen, Dr. K. Y. Amsharov
Max Planck Institute for Solid State Research
Stuttgart (Germany)
E-mail: K.Amsharov@fkf.mpg.de
Dr. A. Kromer, Prof. E. Roduner
Institute of Physical Chemistry, Stuttgart (Germany)
Prof. E. Roduner
University of Pretoria, Republic of South Africa

[**] The authors are grateful to Dr. Jürgen Nuss for collecting X-ray data, Ms. Eva Brücher for SQUID measurements, Mr. Patrick Merz and Mr. Wilhelm Gutjahr for assistance with synthesis.

Supporting information for this article is available on the WWW under http://dx.doi.org/10.1002/anie.201305808.

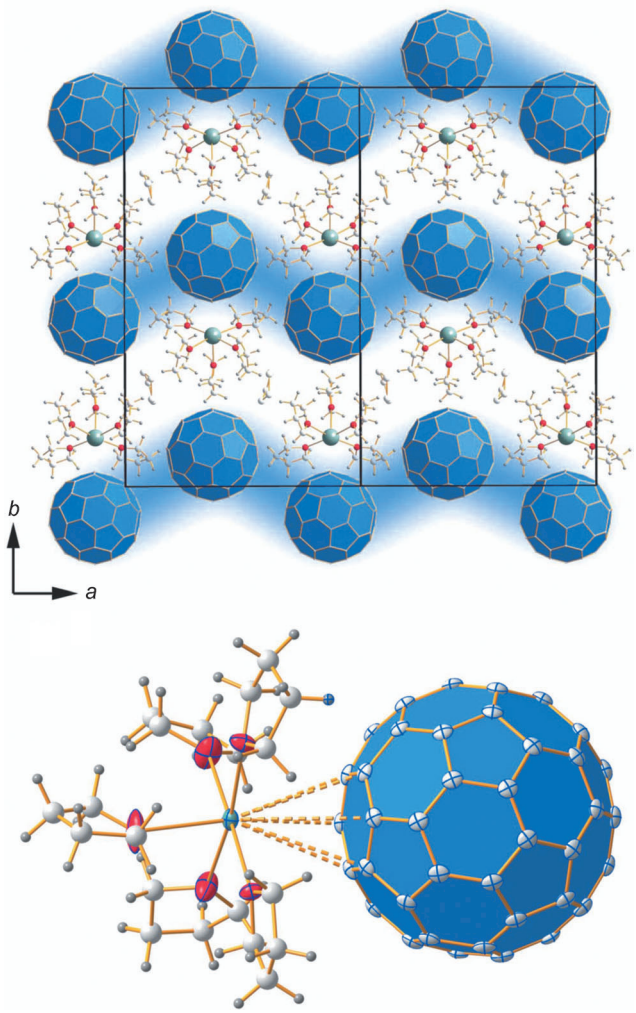

Figure 1. Top panel: Projection of the crystal structure of $KC_{60}(THF)_5 \cdot 2THF$ along the [001] direction showing corrugated layers with short center-to-center fullerene distances in the *a*–*c* crystallographic plane. The layers are highlighted in blue; the unit cell is outlined in black. Bottom panel: Fragment of the crystal structure showing coordination of the potassium cation by THF molecules and fullerene cage (dotted lines). Displacement ellipsoids are drawn at the 50% probability level.

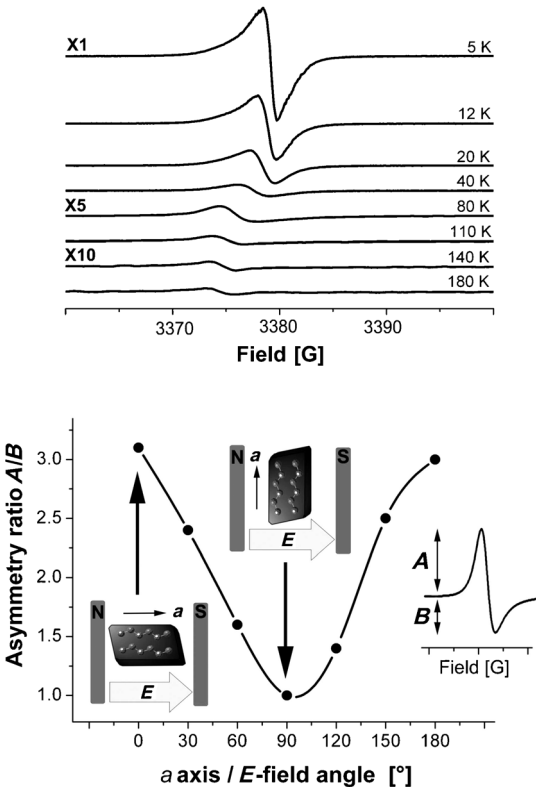

Figure 2. Top panel: ESR spectra observed for a $KC_{60}(THF)_5 \cdot 2THF$ single crystal at various temperatures. The angle between the *a* axis and the static magnetic field is approximately 60°. Bottom panel: Asymmetry parameter *A*/*B* for the Dyson ESR line as a function of rotation of the single crystal at 110 K. (The inset shows the ESR spectrum with *a* axis/magnetic field angle of 60°).

simulation of the resonance with $g = 2.0059$ and a line width of 0.214 mT (20 K) were in good agreement with literature parameters of related systems containing fulleride monoanion radicals.[2,8] As expected, a similar spectral pattern was observed using echo-detected Q-band ESR spectroscopy (see the Supporting Information). In the temperature interval from 40 to 240 K, the ESR signal exhibited an asymmetric Dysonian line shape;[9] in contrast to the normal dispersion lines where the first integral over the resonance is zero, the Dysonian line appeared phase shifted, and the first integral is non-zero. Such a line shape is characteristic for metals and highly conductive materials, and can be attributed to the formation of a skin layer on the single-crystal surface caused by the interaction of charge carriers with the electric field vector of the microwave radiation. As can be seen from Figure 2, the asymmetry ratio of the Dysonian line depended strongly on the relative orientation of the single crystal in the external magnetic field. Rotation of the samples led to a substantial change in the asymmetry parameter. The *A*/*B* ratio maximum was detected at the position of the samples where the crystallographic *a* axis (coincides with the needle axis) was parallel to the electric field of the microwave radiation, whereas the asymmetry completely disappeared when the crystallographic *a* axis was perpendicular to the electric field. Such a behavior indicates the presence of one-dimensional conductivity along the crystallographic *a* axis in $KC_{60}(THF)_5 \cdot 2THF$. This finding is highly unexpected since the intercentroid fullerene–fullerene distances along the *a* axis are remarkably larger (10.15 Å, 100 K) than the ones along the *c* axis (9.85 Å, 100 K). The asymmetry ratio of the Dysonian line (*A*/*B*) versus temperature was recorded with a microwave electric field vector oriented at 45° relative to the crystallographic *a* axis. Below 40 K, no asymmetry of the ESR line was detected. At 40 K the *A*/*B* ratio increased with a rise in temperature, reaching a maximum at 120 K. Further increases in temperature led to the decrease of *A*/*B*, with the asymmetry vanishing completely at 240 K (Figure 3). Interestingly, the temperature dependence of the Dysonian line asymmetry correlates with the intercentroid fullerene–fullerene distances along the conductive *a* axis. The fullerene–fullerene center-to-center distances along the *a* axis reached a minimum at about 120–130 K (Figure 3, blue line) because

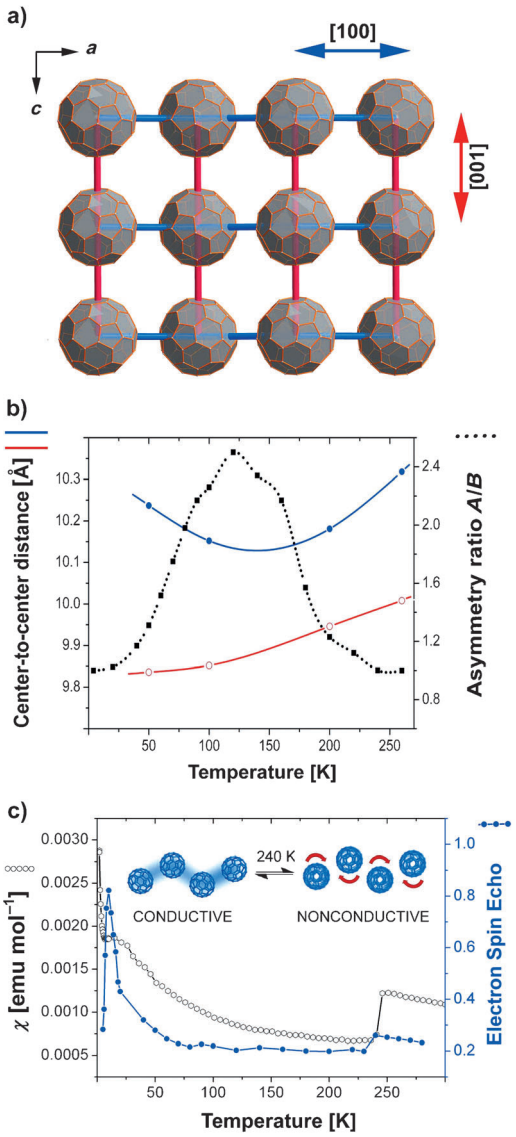

Figure 3. a) Packing of C_{60} radical anions in $KC_{60}(THF)_5{\cdot}2THF$ showing layers in the *a*–*c* plane with short fullerene–fullerene center-to-center distances. Distances are highlighted in blue for the [100] direction and in red for the [001] direction. Note that the layer is corrugated along the *a*-axis. b) Temperature dependence of center-to-center fullerene distances in the fullerene layers (the color code is the same as given in (a); blue and red lines). The black line shows the temperature dependence of the asymmetry ratio *A*/*B* for the Dysonian ESR line (the angle between *a* axis and electric field vector is ca. 45°). c) Temperature dependence of the pulsed Q-band electron spin echo (blue curve) and the SQUID (black curve) magnetization. The phase transition at 240 K leads to ordering of the fullerene anion radicals and formation of conductive fullerene chains (shown schematically in the inset).

of a reduced corrugation of the layers. At this temperature, a more effective interaction of the fullerene anions is realized and the maximum asymmetry ratio of the Dysonian line is observed. This fact additionally confirms the counterintuitive 1D electron transfer along the fullerene channels with larger intercentroid separation instead of conductivity along the *c* axis. Interestingly, a similar decomposition of asymmetric signals for modeling the transition of itinerant to localized spins into normal and Dysonian contributions has been previously observed in conducting carbon nanotubes.[10a]

Magnetic measurements were performed using several single crystals of $KC_{60}(THF)_5{\cdot}2THF$ in the 2–360 K range. Experimental results are compared with those from ESR spectra recorded for an individual single crystal (Figure 3). The main differences between superconducting quantum interference device (SQUID) and ESR magnetization measurements are the applied magnetic field and the amount of the fulleride salt. Below 5 K, a sharp decrease of the spin susceptibility represented by the initial electron spin echo amplitude in Q-band ESR (blue curve in Figure 3c) was observed, the typical fingerprint of an antiferromagnetic phase transition. The same drop of the EPR susceptibility at low temperatures was also observed in conducting carbon nanotubes.[10b] The most probable reason for a low-temperature diamagnetic ground state in $KC_{60}(THF)_5{\cdot}2THF$ as seen by the temperature dependence of the ESR magnetization is the phase-transition mechanism associated with dimerization of the paramagnetic fulleride anions. Because of recombination of two C_{60} anion radicals to diamagnetic $(C_{60})_2^{2-}$, the interaction in the conducting channels in the fullerene layers is broken and the electric conductivity disappears. In accordance with the SQUID measurements at a magnetic field of 10000 G, the starting point of fullerene anion radical recombination was detected at 10 K as well. In the highly conducting range between 40 and 240 K, ESR spectroscopy and magnetic susceptibility were almost temperature independent, about 7.5×10^{-4} emu mol^{-1}, which can be interpreted as a Pauli paramagnetic contribution resulting from the conducting C_{60} channels inside the fullerene layers. The sudden increase in the magnetic susceptibility from 240 K indicates the presence of a second metal-to-insulator transition. The presence of this high-temperature phase transition and the lack of conductivity above 240 K is a result of the onset of rotation of interacting fullerene anions as was determined crystallographically. This strong correlation between the ordering of C_{60} and the physical properties was previously observed in several fullerides.[11] The temperature range of the SQUID measurements over 240–295 K can be fitted using the Curie–Weiss law with diamagnetic corrections $\chi_M = C/(T-\theta)+\chi_0$ with $\theta = -54$ K and $\chi_0 = -3.89\times10^{-4}$ emu mol^{-1}. The Curie–Weiss constant $C = 0.321$ emu K mol^{-1} corresponds to 85% of the total number of spins. Low Curie–Weiss values were observed previously in fullerides.[5,6] This effect can be attributed to antiferromagnetic interactions or to the orientation dependence of the magnetic susceptibility.

To understand this rather unique experimental finding, we further analyzed the band structure of the title compound in the framework of density functional theory (DFT). Depending on the functional used, a small band gap (hybrid functional B3LYP:[12] 0.47 eV) or bands crossing the Fermi level (PBE[13]) resulted. In both cases, however, characteristics of the bands as well as the spin density distributions were very similar. For clarity, B3LYP results are represented in Figure 4 (for corresponding PBE data, see the Supporting Information). The molecular crystal band structure was mainly dominated by the molecular orbital (MO) spectrum of the isolated neutral or charged units. Intermolecular interactions

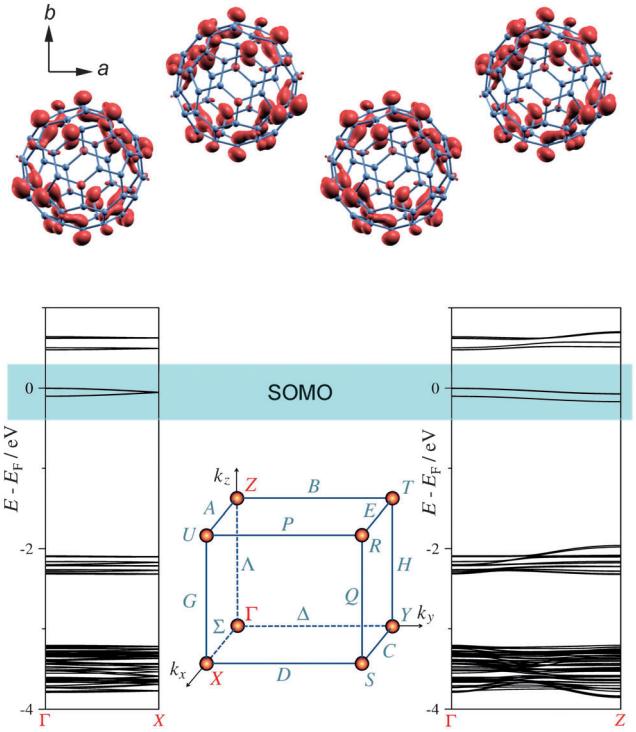

Figure 4. Spin density (top, isosurface at 0.014 e^{-} Å^{-3}) and sections of the band structure of $KC_{60}(THF)_5{\cdot}2\,THF$ (100 K), calculated at the B3LYP level. The band dispersion (majority spin) is represented along the Γ-X-line in the Brillouin zone, corresponding to the *a* axis in position space, and along the Γ-Z-line (*c* axis). The partially filled bands at the Fermi level (0 eV) are highlighted (SOMO in the isolated anion). Details of the Brillouin zone are shown in the inset.

giving rise to the long-range order led to a dispersion of this spectrum in the Brillouin zone. The most pronounced dispersion in $KC_{60}(THF)_5{\cdot}2\,THF$ was found along the Γ-Z-line, which corresponds to the [001] direction in position space and reflects the short intercentroid fullerene–fullerene distances in this direction. A conspicuous exception to this general dispersion trend, however, was found at the partially occupied bands (the singly occupied orbital, SOMO, of the isolated C_{60} anion) at the Fermi level, which mainly determine the conducting behavior of the compound. Here, significant dispersion appeared along Γ-X corresponding to the [100] direction in position space. The long-range interaction between the SOMOs along the *a* axis can be correlated with the 1D conductivity in this direction. The distribution of the spin density, which reflects the shape of the SOMO, gives a hint for the reason of this counterintuitive directional conductivity. As can be seen from Figure 4, the SOMO of the C_{60} anion in the crystal has a node, the plane of which is perpendicular to the *a*–*b* plane. Because of the corrugation along [100], an efficient overlap of the high-amplitude regions becomes possible. Thus, in the temperature region from 40 to 240 K where the intercentroid fullerene–fullerene distances are smaller than 10.2 Å conductivity is observed. Conversely, SOMO overlap is not effective along the *c* axis and therefore no electron transport is observed in this direction, despite the short $C_{60}\cdots C_{60}$ contacts.

In summary, we have synthesized and characterized single crystals of the fulleride-based 1D electric conductor $KC_{60}(THF)_5{\cdot}2\,THF$, in which C_{60} anions are highly ordered in 2D corrugated layers. The combination of a counter alkali metal cation coordinated with solvent ligands prevents the dimerization of $C_{60}^{\bullet-}$, over a large temperature range, thus avoiding losses in conductivity. Moreover, the spatial separation of particular fullerene anions kept their orbital correlations, resulting in 1D conductivity in the 2D layer with counterintuitive anisotropy. On the basis of experimental ESR and SQUID data and X-ray analysis, we have demonstrated that conduction electrons move freely only along the C_{60} channels with a larger intercentroid separation, whereas the channels with shorter C_{60}–C_{60} contacts in the same layer are nonconductive. Quantum chemical calculations reveal that the orientations of fullerene anion radicals play a key role in the effective interaction of the SOMO orbitals along [100] required for the manifestation of the conductivity. It was shown, that electron transport in fullerides heavily depends on the nodal structure of the SOMOs and their orientation. Thus, short intercentroid fullerene–fullerene distances (less than 9.9 Å) are not a sufficient prerequisite for the manifestation of conductivity. However, conductivity may be observed even at large separations (i.e., 10.0–10.2 Å) if the SOMOs interact effectively. In a generalized sense, the findings can be addressed as a consequence of orbital ordering of the SOMO, induced by polarization of the coordinated potassium cations.

Experimental Section

Synthesis of $KC_{60}(THF)_5{\cdot}2\,THF$: 50 mg (0.0069 mmol) of C_{60} (MER Corporation, USA, 99.9%) were reacted with 20 mg (0.0306 mmol) of Zn powder and 10 mg KOH (0.18 mmol) in 12 mL of THF containing 2 mL of *n*-octane and 0.2 mL of water. The reaction mixture was cooled with liquid nitrogen and degassed under vacuum (2×10^{-3} mbar). The reaction was allowed to warm to room temperature and was stirred for 10–20 h, resulting in a dark red-purple solution. The solution of KC_{60} was filtered and used for crystal growth by gradient solvent exchange as described elsewhere.[6] All manipulations were carried out in an all-glass system to exclude any contamination.

Structure determination: For X-ray diffraction experiments, a black needle-like crystal was selected from the sealed-off ampoule, transferred into a highly viscous oil and was attached onto a loop. Intensity data of the single crystal were collected with a Smart APEX II diffractometer (Bruker AXS, Karlsruhe, Germany) with Mo-K_a radiation (0.071073 Å) at different temperatures. Data reduction was carried out with the Bruker Suite software package; absorption correction was applied using SADABS.[14] The structure was solved by direct methods and refined by full-matrix least-squares fitting with the SHELXTL software package.[15] No constraints were used during the structure refinement. The C_{60} molecule was completely ordered at 50, 100, and 200 K. Disordered C_{60} (260 K measurement) was simulated by 120 carbon atoms with 50% occupancy.[16]

Magnetic susceptibility, $\chi(T)$, was recorded on a Quantum Design "MPMS XL" magnetometer at magnetic fields of 0.1, 1.0, and 7.0 T in the temperature region of 2–360 K.

ESR measurements were performed in the 5–298 K range using a Bruker CW X-band spectrometer and home-build pulsed Q-band spectrometer in the 5–298 K range. The crystals were fixed with silicon paste in a Suprasil glass tube of 2 mm outer diameter and

measured immediately after preparation. ESR measurements were carried out for a collection of single-crystal samples with different orientations relative to the external magnetic field. The absolute direction of the *a* axis in the single crystal was determined crystallographically.

DFT calculations with periodic boundary conditions were performed with the CRYSTAL09 program.[17] Two functionals, the hybrid functional B3LYP[12] and the GGA (generalized gradient approximation) functional PBE[13] were applied, together with an atomic basis set of split valence quality. The structures determined experimentally at 50 and 100 K were considered. In the spin-polarized unrestricted Kohn–Sham iterations, 27 *k*-points in the irreducible part of the Brillouin zone were sampled. More details and data can be found in the Supporting Information.

Received: July 4, 2013
Revised: August 20, 2013
Published online: October 2, 2013

Keywords: conductivity · density functional calculations · fullerenes · X-ray diffraction

[1] a) A. F. Hebard, M. J. Rosseinsky, R. C. Haddon, D. W. Murphy, S. H. Glarum, T. T. M. Palstra, A. P. Ramirez, A. R. Kortan, *Nature* **1991**, *350*, 600 – 601; b) K. Tanigaki, O. Zhou, *J. Phys. I* **1996**, *6*, 2159 – 2173; c) O. Gunnarsson, *Rev. Mod. Phys.* **1997**, *69*, 575 – 606; d) M. J. Rosseinsky, *Chem. Mater.* **1998**, *10*, 2665 – 2685; e) S. Margadonna, K. Prassides, *J. Solid State Chem.* **2002**, *168*, 639 – 652; f) A. Y. Ganin, Y. Takabayashi, Y. Z. Khimyak, S. Margadonna, A. Tamai, M. J. Rosseinsky, K. Prassides, *Nat. Mater.* **2008**, *7*, 367.

[2] C. A. Reed, R. D. Bolskar, *Chem. Rev.* **2000**, *100*, 1075 – 1120, and references therein.

[3] a) N. Kozhemyakina, K. Yu. Amsharov, J. Nuss, M. Jansen, *Chem. Eur. J.* **2010**, *16*, 1798 – 1805; b) D. V. Konarev, S. S. Khasanov, G. Saito, A. Otsuka, R. N. Lyubovskaya, *J. Mater. Chem.* **2007**, *17*, 4171 – 4177; c) D. V. Konarev, S. S. Khasanov, G. Saito, A. Otsuka, Y. Yoshida, R. N. Lyubovskaya, *J. Am. Chem. Soc.* **2003**, *125*, 10074 – 10083; d) D. V. Konarev, S. S. Khasanov, A. Otsuka, G. Saito, *J. Am. Chem. Soc.* **2002**, *124*, 8520 – 8521.

[4] a) W. Chou Wan, X. Liu, G. M. Sweeney, W. E. Broderick, *J. Am. Chem. Soc.* **1995**, *117*, 9580 – 9581; b) D. V. Konarev, A. V. Kuzmin, S. V. Simonov, S. S. Khasanov, E. I. Yudanova, R. N. Lyubovskaya, *Dalton Trans.* **2011**, *40*, 4453 – 4458.

[5] D. V. Konarev, S. S. Khasanov, A. Otsuka, M. Maesato, G. Saito, R. N. Lyubovskaya, *Angew. Chem.* **2010**, *122*, 4939 – 4942; *Angew. Chem. Int. Ed.* **2010**, *49*, 4829 – 4832.

[6] K. Yu. Amsharov, Y. Krämer, M. Jansen, *Angew. Chem.* **2011**, *123*, 11844 – 11847; *Angew. Chem. Int. Ed.* **2011**, *50*, 11640 – 11643.

[7] N. V. Kozhemyakina, J. Nuss, M. Jansen, *Z. Anorg. Allg. Chem.* **2009**, *635*, 1355 – 1361.

[8] a) A. Stasko, V. Brezova, P. Rapta, P. Biskupic, K. P. Dinse, A. Gugel, *Res. Chem. Intermed.* **1997**, *23*, 453 – 478; b) X. W. Wei, Z. Y. Suo, G. Yin, Z. Xu, *J. Organomet. Chem.* **2000**, *599*, 69.

[9] a) F. J. Dyson, *Phys. Rev.* **1955**, *98*, 349 – 359; b) G. Feher, A. F. Kip, *Phys. Rev.* **1955**, *98*, 337 – 348.

[10] a) B. Corzilius, A. Gembus, N. Weiden, K.-P. Dinse, K. Hata, *Phys. Status Solidi B* **2006**, *243*, 3273 – 3276; b) B. Corzilius, K.-P. Dinse, J. van Slageren, K. Hata, *Phys. Rev. B* **2007**, *75*, 235416.

[11] a) T. Yildirim, J. E. Fischer, A. B. Harris, P. W. Stephens, D. Liu, L. Brard, R. M. Strongin, A. B. Smith III, *Phys. Rev. Lett.* **1993**, *71*, 1383 – 1386; b) K. Prassides, C. Christides, I. M. Thomas, J. Mizuki, K. Tanigaki, I. Hirosawa, T. W. Ebbesen, *Science* **1994**, *263*, 950 – 954; c) D. Mihailovic, D. Arcon, P. Verturini, R. Blinc, A. Omerzu, P. Cevc, *Science* **1995**, *268*, 400 – 402.

[12] A. D. Becke, *J. Chem. Phys.* **1993**, *98*, 5648 – 5652.

[13] J. P. Becke, K. Burke, M. Ernzerhof, *Phys. Rev. Lett.* **1996**, *77*, 3865 – 3868.

[14] G. M. Sheldrick, *SADABS*—Bruker AXS area detector scaling and absorption, Version 2008/1, University of Göttingen, Germany **2008**.

[15] G. M. Sheldrick, *Acta Crystallogr. Sect. A* **2008**, *64*, 112.

[16] Crystal data: ($T = 100(2)$ K) orthorhombic; space group $P2_12_12$; $a = 17.840(2)$, $b = 30.208(4)$, $c = 9.8517(11)$ Å; $V = 5309.2$ Å^3, $Z = 4$; $2\theta_{max} = 72.0°$; $-29 < h < 29$, $-49 < k < 49$, $-16 < l < 16$; $\lambda = 0.71073$ Å; final R value 0.0668 ($R_w = 0.1854$); ($T = 260(2)$ K) orthorhombic; space group $Pca2_1$; $a = 30.507(13)$, $b = 10.008(4)$, $c = 18.079(8)$ Å; $V = 5520$ Å^3, $Z = 4$; $2\theta_{max} = 39.5°$; $-28 < h < 28$, $-9 < k < 9$, $-17 < l < 17$; $\lambda = 0.71073$ Å; final R value 0.1448 ($R_w = 0.4091$). CCDC 940864, 940865, 940866, 940867 contain the supplementary crystallographic data for this paper. These data can be obtained free of charge from The Cambridge Crystallographic Data Centre via www.ccdc.cam.ac.uk/data_request/cif.

[17] a) R. Dovesi, V. R. Saunders, C. Roetti, R. Orlando, C. M. Zicovich-Wilson, F. Pascale, B. Civalleri, K. Doll, N. M. Harrison, I. J. Bush, P. D'Arco, M. Llunell, *CRYSTAL09 User's Manual*, University of Torino, Torino, **2009**; b) R. Dovesi, R. Orlando, B. Civalleri, C. Roetti, V. R. Saunders, C. M. Zicovich-Wilson, *Z. Kristallogr.* **2005**, *220*, 571 – 573.

